SCIENTIA
Series A: *Mathematical Sciences*, Vol. 13 (2006), 46–56
Universidad Técnica Federico Santa María
Valparaíso, Chile
ISSN 0716-8446

Adaptive solutions of an augmented mixed finite element scheme for linear elasticity

Tomás Barrios

Abstract. Through several numerical experiments, we explore the theoretical properties of a residual based a posteriori error estimator of an augmented mixed method applied to linear elasticity problem in the plane. More precisely, we show numerical evidence confirming the theoretical properties of the estimator, and ilustrating the capability of the corresponding adaptive algorithm to localize the singularities and the large stress regions of the solution.

1. Introduction

In the recent paper [**2**], an augmented mixed finite element method for the linear elasticity was presented and analyzed. The approach used in [**2**] is based on the introduction of suitable Galerkin least-squares terms arising from the constitutive and equilibrium equations, and from the relation defining the rotation in terms of the displacement. This leads to well posed continuous and discrete problems. In particular, the discrete scheme allows the use of simple finite element spaces, such as, Raviart-Thomas spaces of lowest order for the stress tensor, piecewise linear elements for the displacement, and piecewise constants for the rotation, which should be easily generalized to 3D.

On the other hand, since adaptive techniques are particularly necessary for the elasticity problem, we provided in [**1**] a residual based a posteriori error estimator for the augmented approach for the elasticity problem with pure Dirichlet boundary condition in the plane. Specifically, we derives a reliable and efficient a posteriori error estimator.

The purpose of the present work is twofold. First, we want to present a review of a priori and a posteriori error analysis of the augmented mixed formulation applies to linear elasticity problem with pure Dirichlet boundary conditions, and secondly, we show numerical evidence confirming the theoretical properties of the augmented scheme and the corresponding adaptive algorithm based on a posteriori error estimator.

The rest of the paper is organized as follows. In Section 2, 3 and 4, we give a review of the a priori and a posteriori error analysis of the augmented mixed formulation. Finally, several numerical results illustrating the performance of the augmented

2000 *Mathematics Subject Classification.* Primary 65N30, 65N15, 65N12 Secondary 74B05.
Key words and phrases. mixed finite elements, augmented formulation, a posteriori error estimates, linear elasticity .

mixed finite element scheme, and the reliability and efficiency of the a posteriori error estimator, are provided in Section 5.

2. The augmented mixed variational formulation

Let Ω be a simply connected domain in $\mathbb{R}^2$ with polygonal boundary $\partial\Omega$. Given a volume force $\mathbf{f} \in [L^2(\Omega)]^2$, we seek the displacement $\mathbf{u}$ and the stress tensor $\boldsymbol{\sigma}$ such that

$$\boldsymbol{\sigma} = C\mathbf{e}(\mathbf{u}) \quad \text{in } \Omega\,,$$
$$-\,\mathbf{div}\,(\boldsymbol{\sigma}) = \mathbf{f} \quad \text{in } \Omega \quad \mathbf{u} = 0 \quad \text{on } \partial\Omega\,.$$

Here, $\mathbf{e}(\mathbf{u}) := \frac{1}{2}(\nabla\mathbf{u} + (\nabla\mathbf{u})^t)$ is the strain tensor of small deformations and C is the elasticity tensor determined by Hooke's law, that is

$$C\boldsymbol{\zeta} := \lambda tr(\boldsymbol{\zeta})\mathbf{I} + 2\mu\boldsymbol{\zeta} \quad \forall\boldsymbol{\zeta} \in [L^2(\Omega)]^{2\times 2}\,,$$

where λ, $\mu, > 0$ denote the corresponding Lamé constants. The inverse tensor C^{-1} is given by

$$C^{-1}\boldsymbol{\zeta} := \frac{1}{2\mu}\boldsymbol{\zeta} - \frac{\lambda}{4\mu(\lambda+\mu)}tr(\boldsymbol{\zeta})\mathbf{I}\,.$$

In order to introduce the variational formulation we let us define the spaces

$$H(\mathbf{div}\,;\Omega) := \{\boldsymbol{\tau} \in [L^2(\Omega)]^{2\times 2} : \mathbf{div}\,(\boldsymbol{\tau}) \in [L^2(\Omega)]^2\}\,,$$
$$[L^2(\Omega)]^{2\times 2}_{skew} := \{\boldsymbol{\eta} \in [L^2(\Omega)]^{2\times 2} : \boldsymbol{\eta} + \boldsymbol{\eta}^t = 0\}$$

and $H_0 := \{\boldsymbol{\tau} \in H(\mathbf{div}\,;\Omega) : \int_\Omega tr(\boldsymbol{\tau}) = 0\}$. Note that $H = H_0 \oplus \mathbb{R}\mathbf{I}$, that is, for any $\boldsymbol{\tau} \in H$ there exists a unique representation $\boldsymbol{\tau} = \boldsymbol{\tau}_0 + d\mathbf{I}$ with $\boldsymbol{\tau}_0 \in H_0$ and $d = \frac{1}{2|\Omega|}\int_\Omega tr(\boldsymbol{\tau}) \in \mathbb{R}$.

Given positive parameters κ_1, κ_2, κ_3 independent of λ, we obtain, as in [**2**], the following augmented variational formulation: *Find* $(\boldsymbol{\sigma}, \mathbf{u}, \boldsymbol{\gamma}) \in \mathbf{H}_0 := H_0 \times [H^1_0(\Omega)]^2 \times [L^2(\Omega)]^{2\times 2}_{skew}$ *such that*

$$A((\boldsymbol{\sigma}, \mathbf{u}, \boldsymbol{\gamma}), (\boldsymbol{\tau}, \mathbf{v}, \boldsymbol{\eta})) = F(\boldsymbol{\tau}, \mathbf{v}, \boldsymbol{\eta})\,, \tag{2.1}$$

for all $(\boldsymbol{\tau}, \mathbf{v}, \boldsymbol{\eta}) \in \mathbf{H}_0$. Here, the bilinear form $A : \mathbf{H}_0 \times \mathbf{H}_0 \to \mathbb{R}$ and the functional $F : \mathbf{H}_0 \to \mathbb{R}$ are defined by

$$\begin{aligned} A((\boldsymbol{\sigma}, \mathbf{u}, \boldsymbol{\gamma}), (\boldsymbol{\tau}, \mathbf{v}, \boldsymbol{\eta})) &:= \int_\Omega C^{-1}\boldsymbol{\sigma} : \boldsymbol{\tau} + \int_\Omega \mathbf{u} \cdot \mathbf{div}\,(\boldsymbol{\tau}) + \int_\Omega \boldsymbol{\gamma} : \boldsymbol{\tau} - \int_\Omega \mathbf{v} \cdot \mathbf{div}\,(\boldsymbol{\sigma}) \\ &- \int_\Omega \boldsymbol{\eta} : \boldsymbol{\sigma} + \kappa_1 \int_\Omega (\mathbf{e}(\mathbf{u}) - C^{-1}\boldsymbol{\sigma}) : (\mathbf{e}(\mathbf{v}) + C^{-1}\boldsymbol{\tau}) \\ &+ \kappa_2 \int_\Omega \mathbf{div}\,(\boldsymbol{\sigma}) \cdot \mathbf{div}\,(\boldsymbol{\tau}) + \kappa_3 \int_\Omega (\boldsymbol{\gamma} - \frac{1}{2}(\nabla\mathbf{u} - (\nabla\mathbf{u})^t) : (\boldsymbol{\eta} + \frac{1}{2}(\nabla\mathbf{v} - (\nabla\mathbf{v})^t) \end{aligned}$$

and

$$F(\boldsymbol{\tau}, \mathbf{v}, \boldsymbol{\eta}) := \int_\Omega \mathbf{f} \cdot (\mathbf{v} - \kappa_2\,\mathbf{div}\,(\boldsymbol{\tau}))\,.$$

The unique solvability of (2.1) was proved in [**2**]:

THEOREM 2.1. *Assume that* $(\kappa_1, \kappa_2, \kappa_3)$ *is independent of* λ *and such that* $0 < \kappa_1 < 2\,\mu$, $0 < \kappa_2$, *and* $0 < \kappa_3 < \kappa_1$. *Then, there exist positive constants* M, α, *independent of* λ, *such that*

$$|\,A((\boldsymbol{\sigma}, \mathbf{u}, \boldsymbol{\gamma}), (\boldsymbol{\tau}, \mathbf{v}, \boldsymbol{\eta}))\,| \;\leqslant\; M\;\|(\boldsymbol{\sigma}, \mathbf{u}, \boldsymbol{\gamma})\|_{\mathbf{H}_0}\,\|(\boldsymbol{\tau}, \mathbf{v}, \boldsymbol{\eta})\|_{\mathbf{H}_0} \tag{2.2}$$

and

$$A((\boldsymbol{\tau},\mathbf{v},\boldsymbol{\eta}),(\boldsymbol{\tau},\mathbf{v},\boldsymbol{\eta})) \;\geqslant\; \alpha\,\|(\boldsymbol{\tau},\mathbf{v},\boldsymbol{\eta})\|^2_{\mathbf{H}_0} \tag{2.3}$$

for all $(\boldsymbol{\sigma},\mathbf{u},\boldsymbol{\gamma})$, $(\boldsymbol{\tau},\mathbf{v},\boldsymbol{\eta}) \in \mathbf{H}_0$. *In particular, taking*

$$\kappa_1 \,=\, \tilde{C}_1\,\mu\,, \qquad \kappa_2 = \frac{1}{\mu}\,\left(1-\frac{\kappa_1}{2\,\mu}\right), \qquad \textit{and} \qquad \kappa_3 \,=\, \tilde{C}_3\,\kappa_1\,, \tag{2.4}$$

with any $\tilde{C}_1 \in]0,2[$ *and any* $\tilde{C}_3 \in]0,1[$, *this yields* M *and* α *depending only on* μ, $\dfrac{1}{\mu}$, *and* Ω. *Therefore, the augmented variational formulation* (2.1) *has a unique solution* $(\boldsymbol{\sigma},\mathbf{u},\boldsymbol{\gamma}) \in \mathbf{H}_0$, *and there exists a positive constant* C, *independent of* λ, *such that*

$$\|(\boldsymbol{\sigma},\mathbf{u},\boldsymbol{\gamma})\|_{\mathbf{H}_0} \,\leqslant\, C\,\|F\| \,\leqslant\, C\,\|\mathbf{f}\|_{[L^2(\Omega)]^2}\,.$$

Proof. See Theorems 3.1 and 3.2 in [**2**]. □

3. The augmented mixed finite element scheme

By the coercivity and continuity of the bilinear form $A(\cdot,\cdot)$ (see Theorem 2.1), any conforming finite element scheme converges quasi-optimal. In the following we introduce the finite element scheme presented in [**2**].

Let $\{T_h\}_{h>0}$ be a regular family of triangulations of $\bar{\Omega}$ by triangles T of diameter h_T and define, as usual, $h := \max\{\, h_T :\; T \in T_h\,\}$. Given an integer $l \geqslant 0$ and a subset S of $\mathbb{R}^2$, we denote by $\mathbb{P}_l(S)$ the space of polynomials in two variables defined on S of total degree at most l, and for each $T \in T_h$ we put

$$\mathbb{RT}_0(T) := \text{span}\left\{ \begin{pmatrix} 1 \\ 0 \end{pmatrix}, \begin{pmatrix} 0 \\ 1 \end{pmatrix}, \begin{pmatrix} x_1 \\ x_2 \end{pmatrix} \right\},$$

where $x := \begin{pmatrix} x_1 \\ x_2 \end{pmatrix}$ is a generic vector of $\mathbb{R}^2$. We define the Raviart-Thomas space of lowest order

$$H_h^{\boldsymbol{\sigma}} := \{\boldsymbol{\tau}_h \in H(\mathbf{div}\,;\Omega) :\quad \boldsymbol{\tau}_h|_T \in [\mathbb{RT}_0(T)^t]^2 \quad \forall T \in T_h\}$$

and the space of continuous piecewise linear functions

$$\mathbf{H}_h^{\mathbf{u}} := \{\mathbf{v}_h \in [C(\overline{\Omega})]^2 :\quad \mathbf{v}_h|_T \in [\mathbb{P}_1(T)]^2 \quad \forall T \in T_h\}\,.$$

Then the finite element space is $\mathbf{H}_{0,h} := \mathbf{H}_{0,h}^{\boldsymbol{\sigma}} \times H_{0,h}^{\mathbf{u}} \times H_h^{\boldsymbol{\gamma}} \subseteq \mathbf{H}_0 := H_0 \times [H_0^1(\Omega)]^2 \times [L^2(\Omega)]^{2\times 2}_{skew}$, where

$$H_{0,h}^{\boldsymbol{\sigma}} := \left\{\boldsymbol{\tau}_h \in H_h^{\boldsymbol{\sigma}} :\quad \int_\Omega tr(\boldsymbol{\tau}_h) = 0\right\},$$

$$H_{0,h}^{\mathbf{u}} := \{\mathbf{v}_h \in H_h^{\mathbf{u}} :\quad \mathbf{v}_h = 0 \quad \text{on} \quad \partial\Omega\}\,,$$

and

$$H_h^{\boldsymbol{\gamma}} := \left\{\boldsymbol{\eta}_h \in [L^2(\Omega)]^{2\times 2}_{skew} :\quad \boldsymbol{\eta}_h|_T \in [\mathbb{P}_0(T)]^{2\times 2} \quad \forall T \in T_h\right\}.$$

The Galerkin scheme then reads: *Find* $(\boldsymbol{\sigma}_h,\mathbf{u}_h,\boldsymbol{\gamma}_h) \in \mathbf{H}_{0,h}$ *such that*

$$A((\boldsymbol{\sigma}_h,\mathbf{u}_h,\boldsymbol{\gamma}_h),(\boldsymbol{\tau}_h,\mathbf{v}_h,\boldsymbol{\eta}_h)) = F(\boldsymbol{\tau}_h,\mathbf{v}_h,\boldsymbol{\eta}_h) \quad \forall (\boldsymbol{\tau}_h,\mathbf{v}_h,\boldsymbol{\eta}_h) \in \mathbf{H}_{0,h}\,. \tag{3.1}$$

As mentioned above, the Galerkin scheme converges quasi-optimally:

THEOREM 3.1. *Let $\mathbf{H}_{0,h}$ be any finite element subspace of $\mathbf{H}_0$. Then, under the same assumptions of Theorem* 2.1*, the Galerkin scheme* (3.1) *has a unique solution $(\boldsymbol{\sigma}_h, \mathbf{u}_h, \boldsymbol{\gamma}_h) \in \mathbf{H}_{0,h}$, and there exist positive constants C_1, C_2, independent of λ and h, such that*

$$\|(\boldsymbol{\sigma}_h, \mathbf{u}_h, \boldsymbol{\gamma}_h)\|_{\mathbf{H}_0} \leqslant C_1 \|\mathbf{f}\|_{[L^2(\Omega)]^2}$$

and

$$\|(\boldsymbol{\sigma}, \mathbf{u}, \boldsymbol{\gamma}) - (\boldsymbol{\sigma}_h, \mathbf{u}_h, \boldsymbol{\gamma}_h)\|_{\mathbf{H}_0} \leqslant C_2 \inf_{(\boldsymbol{\tau}_h, \mathbf{v}_h, \boldsymbol{\eta}_h) \in \mathbf{H}_{0,h}} \|(\boldsymbol{\sigma}, \mathbf{u}, \boldsymbol{\gamma}) - (\boldsymbol{\tau}_h, \mathbf{v}_h, \boldsymbol{\eta}_h)\|_{\mathbf{H}_0} . \tag{3.2}$$

Furthermore, if $\boldsymbol{\sigma} \in [H^r(\Omega)]^{2\times 2}$, $\mathbf{div}\, \boldsymbol{\sigma} \in [H^r(\Omega)]^2$, $u \in [H^{r+1}(\Omega)]^2$, and $\boldsymbol{\gamma} \in [H^r(\Omega)]^{2\times 2}$ for some $r \in (0, 1]$. Then there exists $C > 0$, independent of h and λ, such that

$$\|(\boldsymbol{\sigma}, \mathbf{u}, \boldsymbol{\gamma}) - (\boldsymbol{\sigma}_h, \mathbf{u}_h, \boldsymbol{\gamma}_h)\|_{\mathbf{H}_0}$$

$$\leqslant C\, h^r \left\{ \|\boldsymbol{\sigma}\|_{[H^r(\Omega)]^{2\times 2}} + \|\,\mathbf{div}\, \boldsymbol{\sigma}\|_{[H^r(\Omega)]^2} + \|\mathbf{u}\|_{[H^{r+1}(\Omega)]^2} + \|\boldsymbol{\gamma}\|_{[H^r(\Omega)]^{2\times 2}} \right\} .$$

PROOF. See Theorem 4.1 and Section 4.1 in [**2**] for more details. □

4. The residual based a posteriori error estimator

In this section we present a residual based a posteriori error estimator developed in [**1**].

First we introduce some notations. Given $T \in T_h$, let $E(T)$ be the set of its edges, and let E_h be the set of all edges of the triangulation T_h. Then we write $E_h = E_h(\Omega) \cup E_h(\partial\Omega)$, where $E_h(\Omega) := \{e \in E_h : \quad e \subseteq \Omega\}$ and $E_h(\partial\Omega) := \{e \in E_h : e \subseteq \partial\Omega\}$. In what follows, h_T and h_e stand for the diameters of the triangle $T \in T_h$ and the edge $e \in E_h$, respectively. Further, given a tensor-valued function $\boldsymbol{\tau} \in [L^2(\Omega)]^{2\times 2}$ defined in Ω, an edge $e \in E(T) \cap E_h(\Omega)$ and the unit tangential vector $\mathbf{t}_T$ along e, let $J[\boldsymbol{\tau}\mathbf{t}_T]$ be the corresponding jump across e, that is, $J[\boldsymbol{\tau}\mathbf{t}_T] := (\boldsymbol{\tau}_T - \boldsymbol{\tau}_{T'})|_e \mathbf{t}_T$, where T' is the other triangle of T_h having e as an edge. Abusing notation, when $e \in E_h(\partial\Omega)$, we also write $J[\boldsymbol{\tau}\mathbf{t}_T] := \boldsymbol{\tau}|_e \mathbf{t}_T$. The tangential vector $\mathbf{t}_T$ is given by $(-\nu_2, \nu_1)^t$ where $\boldsymbol{\nu}_T := (\nu_1, \nu_2)^t$ is the unit outward normal to ∂T. Analogously we define $J[\boldsymbol{\tau}\boldsymbol{\nu}_T]$.

Then, for $(\boldsymbol{\sigma}, \mathbf{u}, \boldsymbol{\gamma}) \in \mathbf{H}_0$ and $(\boldsymbol{\sigma}_h, \mathbf{u}_h, \boldsymbol{\gamma}_h) \in \mathbf{H}_{0,h}$ being the solutions of the continuous and discrete formulations (2.1) and (3.1), respectively, we define an error

indicator θ_T^2 as follows:

$$
\begin{aligned}
\theta_T^2 \;:=\; & \|\mathbf{f}+\mathbf{div}\,(\boldsymbol{\sigma}_h)\|^2_{[L^2(T)]^2} \,+\, \|\boldsymbol{\sigma}_h-\boldsymbol{\sigma}_h^{\mathtt{t}}\|^2_{[L^2(T)]^{2\times 2}} \,+\, \|\boldsymbol{\gamma}_h-\frac{1}{2}(\nabla\mathbf{u}_h-(\nabla\mathbf{u}_h)^{\mathtt{t}})\|^2_{[L^2(T)]^{2\times 2}} \\
& + \; h_T^2\left\{\|\operatorname{curl}(C^{-1}\boldsymbol{\sigma}_h+\boldsymbol{\gamma}_h)\|^2_{[L^2(T)]^2} \,+\, \|\operatorname{curl}(C^{-1}(\mathbf{e}(\mathbf{u}_h)-C^{-1}\boldsymbol{\sigma}_h))\|^2_{[L^2(T)]^2}\right\} \\
& + \sum_{e\in E(T)} h_e\left\{\|J[(C^{-1}\boldsymbol{\sigma}_h-\nabla\mathbf{u}_h+\boldsymbol{\gamma}_h)\mathbf{t}_T]\|^2_{[L^2(e)]^2} \,+\, \|J[(C^{-1}(\mathbf{e}(\mathbf{u}_h)-C^{-1}\boldsymbol{\sigma}_h))\mathbf{t}_T]\|^2_{[L^2(e)]^2}\right\} \\
& + \; h_T^2\,\|\mathbf{div}\,(\mathbf{e}(\mathbf{u}_h)-\frac{1}{2}(C^{-1}\boldsymbol{\sigma}_h+(C^{-1}\boldsymbol{\sigma}_h)^{\mathtt{t}}))\|^2_{[L^2(T)]^2} \\
& + \; h_T^2\,\|\mathbf{div}\,(\boldsymbol{\gamma}_h-\frac{1}{2}(\nabla\mathbf{u}_h-(\nabla\mathbf{u}_h)^{\mathtt{t}}))\|^2_{[L^2(T)]^2} \\
& + \sum_{e\in E(T)\cap E_h(\Omega)} h_e\,\|J[(\mathbf{e}(\mathbf{u}_h)-\frac{1}{2}(C^{-1}\boldsymbol{\sigma}_h+(C^{-1}\boldsymbol{\sigma}_h)^{\mathtt{t}}))\boldsymbol{\nu}_T]\|^2_{[L^2(e)]^2} \\
& + \sum_{e\in E(T)\cap E_h(\Omega)} h_e\,\|J[(\boldsymbol{\gamma}_h-\frac{1}{2}(\nabla\mathbf{u}_h-(\nabla\mathbf{u}_h)^{\mathtt{t}}))\boldsymbol{\nu}_T]\|^2_{[L^2(e)]^2}\,.
\end{aligned}
\tag{4.1}
$$

As usual, the expression $\boldsymbol{\theta}:=\left(\sum_{T\in T_h}\theta_T^2\right)^{1/2}$ is used as error estimator.

The following theorem establishing the reliability and efficiency of the estimator.

THEOREM 4.1. *Let $(\boldsymbol{\sigma},\mathbf{u},\boldsymbol{\gamma})\in\mathbf{H}_0$ and $(\boldsymbol{\sigma}_h,\mathbf{u}_h,\boldsymbol{\gamma}_h)\in\mathbf{H}_{0,h}$ be the solutions of (2.1) and (3.1), respectively. Then there exist $C_{\mathtt{eff}},C_{\mathtt{rel}}>0$, independent of h and λ, such that*

$$
C_{\mathtt{eff}}\,\boldsymbol{\theta}\;\leqslant\;\|(\boldsymbol{\sigma}-\boldsymbol{\sigma}_h,\mathbf{u}-\mathbf{u}_h,\boldsymbol{\gamma}-\boldsymbol{\gamma}_h)\|_{\mathbf{H}_0}\;\leqslant\;C_{\mathtt{rel}}\,\boldsymbol{\theta}\,.
\tag{4.2}
$$

PROOF. See Theorem 3.1 in [**1**] for details. □

5. Numerical results

In this section we present several numerical results illustrating the performance of the augmented mixed finite element scheme (3.1) and the a posteriori error estimator $\boldsymbol{\theta}$. To this end, in order to implement the integral mean zero condition for functions of the space $H^{\boldsymbol{\sigma}}_{0,h}=\{\boldsymbol{\tau}_h\in H^{\boldsymbol{\sigma}}_h:\quad\int_\Omega tr(\boldsymbol{\tau}_h)=0\}$, in virtue of Theorem 4.3 in [**2**], we consider the equivalent problem: *Find* $(\boldsymbol{\sigma}_h,\mathbf{u}_h,\boldsymbol{\gamma}_h,\varphi_h)\in H^{\boldsymbol{\sigma}}_h\times H^{\mathbf{u}}_{0,h}\times H^{\boldsymbol{\gamma}}_h\times\mathbb{R}$ *such that*

$$
\begin{aligned}
A((\boldsymbol{\sigma}_h,\mathbf{u}_h,\boldsymbol{\gamma}_h),(\boldsymbol{\tau}_h,\mathbf{v}_h,\boldsymbol{\eta}_h))+\varphi_h\int_\Omega tr(\boldsymbol{\tau}_h) &= F(\boldsymbol{\tau}_h,\mathbf{v}_h,\boldsymbol{\eta}_h)\,, \\
\psi_h\int_\Omega tr(\boldsymbol{\sigma}_h) &= 0\,,
\end{aligned}
\tag{5.1}
$$

for all $(\boldsymbol{\tau}_h,\mathbf{v}_h,\boldsymbol{\eta}_h,\psi_h)\in H^{\boldsymbol{\sigma}}_h\times H^{\mathbf{u}}_{0,h}\times H^{\boldsymbol{\gamma}}_h\times\mathbb{R}$.

In what follows, N stands for the total number of degrees of freedom (unknowns) of (5.1), which, at least for uniform refinements, behaves asymptotically as five times

the number of elements of each triangulation (see [**2**]). Also, the individual and total errors are denoted by

$$e(\boldsymbol{\sigma}) := \|\boldsymbol{\sigma} - \boldsymbol{\sigma}_h\|_{H(\mathbf{div};\Omega)}\,, \quad e(\mathbf{u}) := |\mathbf{u} - \mathbf{u}_h|_{[H^1(\Omega)]^2}\,, \quad e(\boldsymbol{\gamma}) := \|\boldsymbol{\gamma} - \boldsymbol{\gamma}_h\|_{[L^2(\Omega)]^{2\times 2}}\,,$$

and

$$e(\boldsymbol{\sigma}, \mathbf{u}, \boldsymbol{\gamma}) := \left\{ [e(\boldsymbol{\sigma})]^2 + [e(\mathbf{u})]^2 + [e(\boldsymbol{\gamma})]^2 \right\}^{1/2}\,,$$

respectively, whereas the effectivity index with respect to $\boldsymbol{\theta}$ is defined by $e(\boldsymbol{\sigma}, \mathbf{u}, \boldsymbol{\gamma})/\boldsymbol{\theta}$.

On the other hand, we recall that given the Young modulus E and the Poisson ratio ν of a linear elastic material, the corresponding Lamé constants are defined by $\mu := \frac{E}{2(1+\nu)}$ and $\lambda := \frac{E\,\nu}{(1+\nu)\,(1-2\,\nu)}$. Then, in order to emphasize the robustness of the a posteriori error estimator $\boldsymbol{\theta}$ with respect to the Poisson ratio, in the examples below we fix $E = 1$ and consider $\nu = 0.4900$, $\nu = 0.4999$, or both, which yield the following values of μ and λ :

ν	μ	λ
0.4900	0.3356	16.4430
0.4999	0.3333	1666.4444

In addition, since the augmented method was already shown in [**2**] to be robust with respect to the parameters κ_1, κ_2, and κ_3, we simply consider for all the examples $(\kappa_1, \kappa_2, \kappa_3) = \left(\mu, \frac{1}{2\,\mu}, \frac{\mu}{2}\right)$, which corresponds to the feasible choice described in Theorem 2.1 with $\tilde{C}_1 = 1$ and $\tilde{C}_3 = \frac{1}{2}$.

We now specify the data of the three examples to be presented here. We take Ω as either the square $]0,1[^2$ or the L-shaped domain $]-0.5,0.5[^2 \setminus [0,0.5]^2$, and choose the datum $\mathbf{f}$ so that ν and the exact solution $\mathbf{u}(x_1, x_2) := (u_1(x_1, x_2), u_2(x_1, x_2))^{\mathtt{t}}$ are given in the table below.

Example	Ω	ν	$u_1(x_1, x_2) = u_2(x_1, x_2)$
1	$]0,1[^2$	0.4900 0.4999	$\sin(\pi\,x_1)\,\sin(\pi\,x_2)$
2	$]-0.5,0.5[^2 \setminus [0,0.5]^2$	0.4900	$\frac{x_1\,x_2\,(x_1^2-0.25)\,(x_2^2-0.25)}{(x_2^2+0.0001)^{1/3}}$
3	$]-0.5,0.5[^2 \setminus [0,0.5]^2$	0.4900	$\frac{x_1\,x_2\,(x_1^2-0.25)\,(x_2^2-0.25)}{(x_1^2+x_2^2)^{1/4}}$

We observe that the solution of Example 3 is singular at the boundary point $(0,0)$. In fact, the behaviour of $\mathbf{u}$ in a neighborhood of the origin implies that $\mathbf{div}\,(\boldsymbol{\sigma}) \in [H^{1/2}(\Omega)]^2$ only, which, according to Theorem 3.1, yields $1/2$ as the expected rate of convergence for the uniform refinement. On the other hand, the solutions of Example 2 and 3 show large stress regions in a neighborhood around the line $x_2 = 0$, and in a neighborhood of the boundary point $(0,0)$, respectively.

The numerical results given below were obtained using a *Compaq Alpha ES40 Parallel Computer* and a Fortran 90 code. The linear system arising from the augmented mixed scheme (5.1) is implemented as explained in Section 4.3 of [**2**], and the individual errors are computed on each triangle using a Gaussian quadrature rule.

We first utilize Example 1 to illustrate the good behaviour of the a posteriori error estimator $\boldsymbol{\theta}$ in a sequence of uniform meshes generated by equally spaced partitions on the sides of the square $]0,1[^2$. In Tables 5.1 and 5.2 we present the individual and total errors, the a posteriori error estimators, and the effectivity indexes for this example, with $\nu = 0.4900$ and $\nu = 0.4999$, for this sequence of uniform meshes. We remark that in this case, and independently of how large the errors could become, there are practically no differences between the effectivity indexes obtained with the two values of ν, which numerically shows the robustness of $\boldsymbol{\theta}$ with respect to the Poisson ratio (and hence with respect to the Lamé constant λ). Moreover, this index remains always in a neighborhood of 0.44, which confirms the reliability and efficiency of $\boldsymbol{\theta}$.

Next, to illustrate the performance of the adaptive algorithm based on $\boldsymbol{\theta}$, which use a parameter $\gamma \in]0,1[$ and *blue-green* procedure to refine (see [**3**] for more details), we consider Example 2 and 3, with parameter $\gamma = \frac{1}{2}$. At this point we introduce the experimental rate of convergence, which, given two consecutive triangulations with degrees of freedom N and N' and corresponding total errors e and e', is defined by

$$r(e) := -2\,\frac{\log(e/e')}{\log(N/N')}\,.$$

In Tables 5.3 through 5.6 we provide the individual and total errors, the experimental rates of convergence, the a posteriori error estimators, and the effectivity indexes for the uniform and adaptive refinements as applied to Examples 2 and 3. In this case, uniform refinement means that, given a uniform initial triangulation, each subsequent mesh is obtained from the previous one by dividing each triangle into the four ones arising when connecting the midpoints of its sides. We observe from these tables that the errors of the adaptive procedure decrease much faster than those obtained by the uniform one, which is confirmed by the experimental rates of convergence provided there. This fact can also be seen in Figures 5.1 and 5.2, where we display the total error $e(\boldsymbol{\sigma}, \mathbf{u}, \boldsymbol{\gamma})$ vs. the degrees of freedom N for both refinements. As shown by the values of $r(e)$, particularly in Example 3 (where $r(e)$ approaches $1/2$ for the uniform refinement), the adaptive method is able to recover, at least approximately, the quasi-optimal rate of convergence $O(h)$ for the total error. Furthermore, the effectivity indexes remain again bounded from above and below, which confirms the reliability and efficiency of $\boldsymbol{\theta}$ for the adaptive algorithm. On the other hand, some intermediate meshes obtained with the adaptive refinement are displayed in Figures 5.3 and 5.4. Note that the method is able to recognize the singularities and the large stress regions of the solutions. In particular, this fact is observed in Example 2 (see Figure 5.3) where the adapted meshes are highly refined around the singular region $x_2 = 0$. Similarly, the adapted meshes obtained in Examples 3 (see Figures 5.4) concentrate the refinements around the boundary point $(0,0)$, where the largest stresses occur.

Summarizing, the numerical results presented in this section underline the reliability and efficiency of $\boldsymbol{\theta}$ and strongly demonstrate that the associated adaptive algorithm is much more suitable than a uniform discretization procedure when solving problems with non-smooth solutions.

Table 5.1: Mesh sizes, individual and total errors, a posteriori error estimators, and effectivity indexes for a sequence of uniform meshes (EXAMPLE 1, $\nu = 0.4900$).

N	h	$e(\boldsymbol{\sigma})$	$e(\mathbf{u})$	$e(\boldsymbol{\gamma})$	$e(\boldsymbol{\sigma},\mathbf{u},\boldsymbol{\gamma})$	$\boldsymbol{\theta}$	$e(\boldsymbol{\sigma},\mathbf{u},\boldsymbol{\gamma})/\boldsymbol{\theta}$
163	0.25000	0.3321E+2	0.2981E+1	0.1116E+1	0.3336E+2	0.1082E+3	0.3081
363	0.16667	0.2224E+2	0.1484E+1	0.6155E+0	0.2230E+2	0.6638E+2	0.3359
643	0.12500	0.1671E+2	0.9399E+0	0.3978E+0	0.1674E+2	0.4686E+2	0.3572
1003	0.10000	0.1337E+2	0.6763E+0	0.2822E+0	0.1339E+2	0.3586E+2	0.3736
1443	0.08333	0.1115E+2	0.5251E+0	0.2133E+0	0.1116E+2	0.2890E+2	0.3864
1963	0.07143	0.9562E+1	0.4285E+0	0.1689E+0	0.9574E+1	0.2413E+2	0.3967
2563	0.06250	0.8369E+1	0.3617E+0	0.1385E+0	0.8377E+1	0.2067E+2	0.4052
3243	0.05556	0.7440E+1	0.3130E+0	0.1166E+0	0.7447E+1	0.1806E+2	0.4123
4003	0.05000	0.6696E+1	0.2720E+0	0.1004E+0	0.6703E+1	0.1602E+2	0.4183
4843	0.04545	0.6088E+1	0.2469E+0	0.8795E-1	0.6093E+1	0.1438E+2	0.4235
5763	0.04167	0.5581E+1	0.2234E+0	0.7810E-1	0.5586E+1	0.1305E+2	0.4279
6763	0.03846	0.5151E+1	0.2041E+0	0.7016E-1	0.5156E+1	0.1193E+2	0.4319
7843	0.03571	0.4784E+1	0.1879E+0	0.6364E-1	0.4788E+1	0.1099E+2	0.4353
9003	0.03333	0.4465E+1	0.1741E+0	0.5821E-1	0.4469E+1	0.1019E+2	0.4384
10243	0.03125	0.4186E+1	0.1623E+0	0.5362E-1	0.4189E+1	0.9495E+1	0.4412
11563	0.02941	0.3940E+1	0.1520E+0	0.4969E-1	0.3943E+1	0.8887E+1	0.4437
12963	0.02777	0.3721E+1	0.1429E+0	0.4630E-1	0.3724E+1	0.8351E+1	0.4459

Table 5.2: Mesh sizes, individual and total errors, a posteriori error estimators, and effectivity indexes for a sequence of uniform meshes (EXAMPLE 1, $\nu = 0.4999$).

N	h	$e(\boldsymbol{\sigma})$	$e(\mathbf{u})$	$e(\boldsymbol{\gamma})$	$e(\boldsymbol{\sigma},\mathbf{u},\boldsymbol{\gamma})$	$\boldsymbol{\theta}$	$e(\boldsymbol{\sigma},\mathbf{u},\boldsymbol{\gamma})/\boldsymbol{\theta}$
163	0.25000	0.3242E+4	0.2631E+3	0.1139E+3	0.3255E+4	0.1066E+5	0.3050
363	0.16667	0.2171E+4	0.1202E+3	0.6320E+2	0.2175E+4	0.6538E+4	0.3327
643	0.12500	0.1631E+4	0.6961E+2	0.4017E+2	0.1633E+4	0.4612E+4	0.3540
1003	0.10000	0.1305E+4	0.4582E+2	0.2773E+2	0.1306E+4	0.3528E+4	0.3704
1443	0.08333	0.1088E+4	0.3264E+2	0.2028E+2	0.1089E+4	0.2841E+4	0.3833
1963	0.07143	0.9334E+3	0.2453E+2	0.1548E+2	0.9338E+3	0.2371E+4	0.3937
2563	0.06250	0.8168E+3	0.1917E+2	0.1221E+2	0.8171E+3	0.2031E+4	0.4023
3243	0.05556	0.7261E+3	0.1542E+2	0.9892E+1	0.7264E+3	0.1773E+4	0.4095
4003	0.05000	0.6536E+3	0.1269E+2	0.8182E+1	0.6537E+3	0.1523E+4	0.4155
4843	0.04545	0.5942E+3	0.1064E+2	0.6885E+1	0.5943E+3	0.1412E+4	0.4208
5763	0.04167	0.5447E+3	0.9062E+1	0.5878E+1	0.5448E+3	0.1280E+4	0.4253
6763	0.03846	0.5028E+3	0.7814E+1	0.5081E+1	0.5029E+3	0.1171E+4	0.4293
7843	0.03571	0.4669E+3	0.6811E+1	0.4437E+1	0.4670E+3	0.1078E+4	0.4328
9003	0.03333	0.4358E+3	0.5993E+1	0.3910E+1	0.4358E+3	0.9997E+3	0.4360
10243	0.03125	0.4085E+3	0.5316E+1	0.3474E+1	0.4086E+3	0.9312E+3	0.4388
11563	0.02941	0.3845E+3	0.4750E+1	0.3107E+1	0.3846E+3	0.8714E+3	0.4413
12963	0.02777	0.3632E+3	0.4271E+1	0.2797E+1	0.3632E+3	0.8187E+3	0.4436

Table 5.3: Individual and total errors, experimental rates of convergence, a posteriori error estimators, and effectivity indexes for the uniform refinement (EXAMPLE 2).

N	$e(\boldsymbol{\sigma})$	$e(\mathbf{u})$	$e(\boldsymbol{\gamma})$	$e(\boldsymbol{\sigma},\mathbf{u},\boldsymbol{\gamma})$	$r(e)$	$\boldsymbol{\theta}$	$e(\boldsymbol{\sigma},\mathbf{u},\boldsymbol{\gamma})/\boldsymbol{\theta}$
123	0.1399E+2	0.4611E+0	0.1636E+0	0.1400E+2	—	0.1449E+2	0.9660
483	0.2522E+2	0.2897E+0	0.1568E+0	0.2522E+2	—	0.2527E+2	0.9978
1923	0.2494E+2	0.1355E+0	0.1448E+0	0.2494E+2	0.0161	0.2495E+2	0.9993
7683	0.1449E+2	0.6382E-1	0.1739E+0	0.1449E+2	0.7841	0.1452E+2	0.9982

Table 5.4: Individual and total errors, experimental rates of convergence, a posterior error estimators, and effectivity indexes for the adaptive refinement (EXAMPLE 2).

N	$e(\boldsymbol{\sigma})$	$e(\mathbf{u})$	$e(\boldsymbol{\gamma})$	$e(\boldsymbol{\sigma},\mathbf{u},\boldsymbol{\gamma})$	$r(e)$	$\boldsymbol{\theta}$	$e(\boldsymbol{\sigma},\mathbf{u},\boldsymbol{\gamma})/\boldsymbol{\theta}$
123	0.1399E+2	0.4611E+0	0.1636E+0	0.1400E+2	——	0.1449E+2	0.9660
263	0.2524E+2	0.3049E+0	0.1386E+0	0.2524E+2	——	0.2533E+2	0.9963
513	0.2498E+2	0.1994E+0	0.1270E+0	0.2498E+2	0.0309	0.2505E+2	0.9972
988	0.1507E+2	0.2016E+0	0.1882E+0	0.1507E+2	1.5421	0.1519E+2	0.9921
2383	0.8490E+1	0.1973E+0	0.1920E+0	0.8494E+1	1.3024	0.8593E+1	0.9884
4038	0.6956E+1	0.1587E+0	0.1468E+0	0.6959E+1	0.7558	0.7061E+1	0.9856
7918	0.5364E+1	0.1592E+0	0.1232E+0	0.5368E+1	0.7709	0.5458E+1	0.9834
12778	0.4268E+1	0.1458E+0	0.1107E+0	0.4272E+1	0.9543	0.4327E+1	0.9872

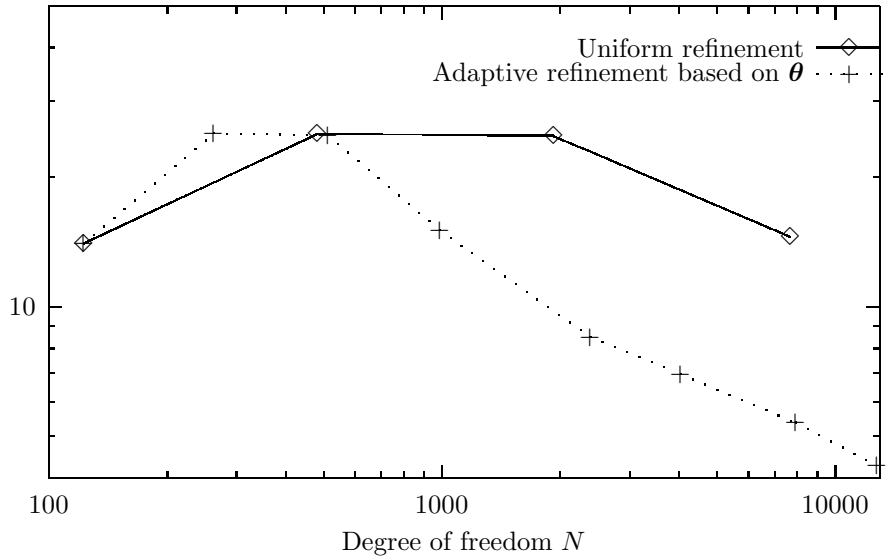

Figure 5.1: Total errors $e(\boldsymbol{\sigma},\mathbf{u},\boldsymbol{\gamma})$ vs. degrees of freedom N for the uniform and adaptive refinements (EXAMPLE 2).

Table 5.5: Individual and total errors, experimental rates of convergence, a posteriori error estimators, and effectivity indexes for the uniform refinement (EXAMPLE 3).

N	$e(\boldsymbol{\sigma})$	$e(\mathbf{u})$	$e(\boldsymbol{\gamma})$	$e(\boldsymbol{\sigma},\mathbf{u},\boldsymbol{\gamma})$	$r(e)$	$\boldsymbol{\theta}$	$e(\boldsymbol{\sigma},\mathbf{u},\boldsymbol{\gamma})/\boldsymbol{\theta}$
123	0.1505E+1	0.1705E+0	0.7587E-1	0.1516E+1	——	0.2251E+1	0.6738
483	0.8993E+0	0.7468E-1	0.8177E-1	0.9061E+0	0.7533	0.1254E+1	0.7223
1923	0.5514E+0	0.3097E-1	0.6290E-1	0.5558E+0	0.7074	0.7066E+0	0.7865
7683	0.3541E+0	0.1836E-1	0.3847E-1	0.3566E+0	0.6405	0.4156E+0	0.8582

Table 5.6: Individual and total errors, experimental rates of convergence, a posteriori error estimators, and effectivity indexes for the adaptive refinement (EXAMPLE 3).

N	$e(\boldsymbol{\sigma})$	$e(\mathbf{u})$	$e(\boldsymbol{\gamma})$	$e(\boldsymbol{\sigma},\mathbf{u},\boldsymbol{\gamma})$	$r(e)$	$\boldsymbol{\theta}$	$e(\boldsymbol{\sigma},\mathbf{u},\boldsymbol{\gamma})/\boldsymbol{\theta}$
123	0.1505E+1	0.1705E+0	0.7587E-1	0.1516E+1	——	0.2251E+1	0.6738
483	0.8993E+0	0.7468E-1	0.8177E-1	0.9061E+0	0.7525	0.1254E+1	0.7223
543	0.8201E+0	0.7105E-1	0.7832E-1	0.8268E+0	1.5643	0.1174E+1	0.7036
1168	0.6416E+0	0.5649E-1	0.5016E-1	0.6460E+0	0.6443	0.7954E+0	0.8122
1628	0.5109E+0	0.4913E-1	0.5098E-1	0.5158E+0	1.3556	0.6623E+0	0.7788
2033	0.4283E+0	0.5125E-1	0.5214E-1	0.4345E+0	1.5441	0.5911E+0	0.7349
2703	0.3826E+0	0.5260E-1	0.5036E-1	0.3895E+0	0.7676	0.5171E+0	0.7533
3898	0.3383E+0	0.6197E-1	0.4422E-1	0.3468E+0	0.6343	0.4301E+0	0.8063
6553	0.2555E+0	0.6762E-1	0.4636E-1	0.2683E+0	0.9881	0.3357E+0	0.7992
7933	0.2282E+0	0.5852E-1	0.4437E-1	0.2397E+0	1.1796	0.3058E+0	0.7840
11398	0.2015E+0	0.5833E-1	0.4187E-1	0.2139E+0	0.6284	0.2626E+0	0.8147

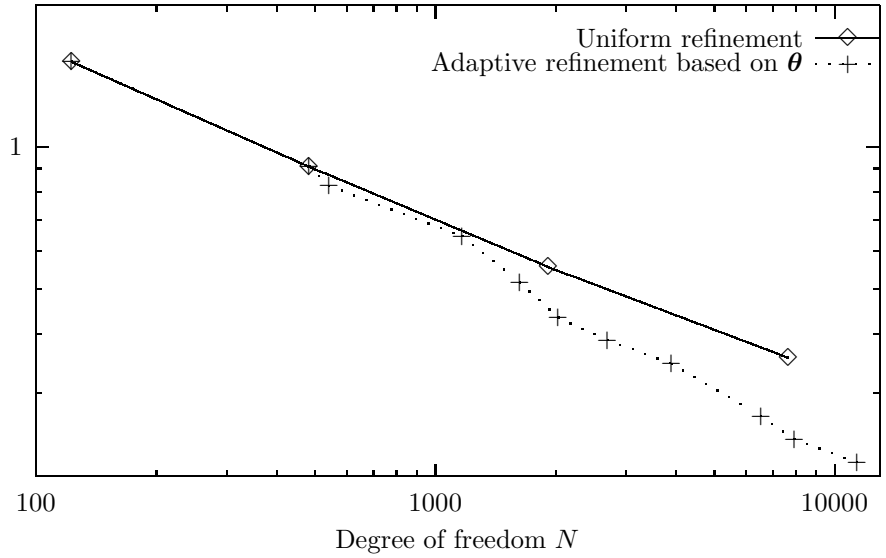

Figure 5.2: Total errors $e(\boldsymbol{\sigma},\mathbf{u},\boldsymbol{\gamma})$ vs. degrees of freedom N for the uniform and adaptive refinements (EXAMPLE 3).

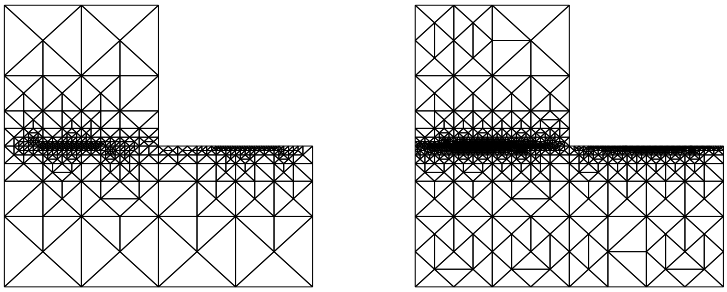

Figure 5.3: Adapted intermediate meshes with 4038 and 12778 degrees of freedom (Example 2).

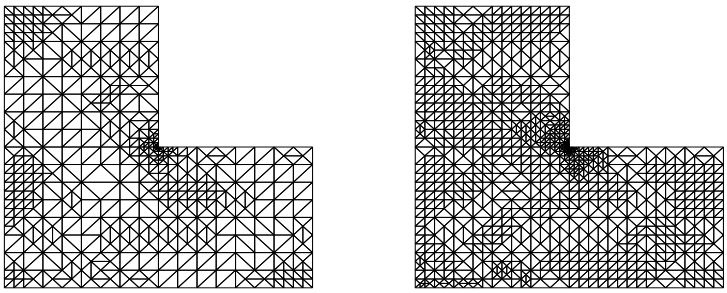

Figure 5.4: Adapted intermediate meshes with 6553 and 11398 degrees of freedom (Example 3).

References

[1] T.P. Barrios, G.N. Gatica, M. González and N. Heuer, *A residual based a posteriori error estimator for an augmented mixed finite element method in linear elasticity.* ESAIM: Mathematical Modelling and Numerical Analysis (2006). To appear.

[2] G.N. Gatica, *Analysis of a new augmented mixed finite element for linear elasticity allowing $RT_0 - P_1 - P_0$ approximations*, ESAIM: Mathematical Modelling and Numerical Analysis, vol. 40, 1, pp. 1-28, (2006).

[3] R. Verfürth, *A Review of A Posteriori Error Estimation and Adaptive Mesh-Refinement Techniques.* Wiley-Teubner (Chichester), 1996.

Received 03 05 2006, revised 15 06 2006

Facultad de Ingeniería,
Universidad Católica de la Santísima Concepción,
Casilla 297, Concepción, Chile.
E-mail address: tomas@ucsc.cl